Progress In Electromagnetics Research C, Vol. 109, 95–110, 2021

Quasi-Static Analysis of Scattering from a Metallic Sphere Coated by Radially Anisotropic Material

Muhammad Yousaf Iqbal*, Aijaz Ali, and Qaisar Abbas Naqvi

Abstract—Theoretical investigation of optical properties of a metallic sphere coated with uniform layer of anisotropic dielectric material is conducted by studying its polarizability, scattering cross section, absorption, and extinction cross section. The dispersive characteristics of metal (tungsten/silver/gold) are mathematically modeled through well known Lorentz-Drude model. A detailed analysis of the behaviors of polarizability, scattering cross-section, absorption, and extinction cross section is carried out for different specific values of the radius and components of the tensor permittivity. The impact of variation of different parameters on location and magnitude of the surface plasmon resonance is highlighted.

1. INTRODUCTION

The scattering of light is ubiquitous in nature; the brightness of the sky and its changing colors are produced due to scattering of light from small particles present in the atmosphere. The exact solution for scattering of electromagnetic waves from spherical objects has been presented in [1] under the Mie theory. Less complicated cases, for instance when the size of the particle is considerably smaller than the wavelength of incident light, can be dealt with using the Rayleigh scattering theory. The scattering of light from nanoparticles has attracted the attention of many researchers due to its modifiable features and numerous applications [2, 3]. The phenomenon of surface plasmon is a major cause of this attention. The surface plasmon resonance (SPR) has been achieved for particles having small size as compared to operating wavelength [4]. SPR has attracted notice [5] of researchers owing to its features in controlling the scattering of light. The study of nanoparticles in this respect has triggered investigations in optics and plasmonics as solar cells [6], biophotonics [7], surface enhanced Raman scattering (SERS) [8], drug targeting [9], plasmonic sensors [10], and bio-sensing [11]. The optical properties of spherical core-shell nanoparticles are associated with their SPR response that can be easily adjusted by varying size, shape, geometry, and the environment of nanoparticles [12, 13]. For example, metallo-dielectric nanoparticle has the ability to manipulate and tune the SPR response [14, 15]. The real metals provide negative permittivity over a wide range of wavelength to produce SPR response. In fact, the majority of solid materials in nature are anisotropic, and radial anisotropy is found in many of these structures [16, 17]. At present, radially anisotropic materials play a very important role in the field of plasmonics [18, 19]. The radially anisotropic materials are used not only to cloak and magnify but also to control plasmonic resonance, scattering, and anomalous absorption of light [20–22]. These interesting applications of radially anisotropic materials incite further curiosity among the researchers.

In present communication, we aim to analyze the scattering cross-section, behaviors of polarizability, extinction cross section, and absorption considering the metallic core covered with a uniform layer of anisotropic medium and placed in unbounded dielectric medium with scalar permittivity. The behavior of polarizability and scattering cross-section for geometry having

Received 19 June 2020, Accepted 19 January 2021, Scheduled 26 January 2021
* Corresponding author: Muhammad Yousaf Iqbal (miqbal@ele.qau.edu.pk).
The authors are with the Department of Electronics, Quaid-i-Azam University, Islamabad, Pakistan.

tungsten/silver/gold metal in core has been studied taking operating wavelength ranging from 800 nm to 3000 nm. These metals are dispersive in nature, and the wavelength dependent dielectric function for mentioned metals has been obtained by the Lorentz-Drude model. The behavior of polarizability and scattering cross-section for spherical geometry have been analyzed for variation in radius of the core and radius of the spherical geometry. Apart from this, the impact of variation of tangential and radial components of permittivity of coated layer has also been analyzed.

2. MATHEMATICAL FORMULATION

Consider that a metallic sphere is coated with an anisotropic dielectric material and is placed in an unbounded dielectric medium as shown in Figure 1. The constitutive parameters of the host medium and medium filling the core are (ϵ_h, μ_0) and (ϵ_1, μ_0), respectively. The tensor form of the permittivity for the anisotropic medium is written below [21–25]

$$\bar{\bar{\epsilon}} = \epsilon_0[\epsilon_{rad} u_r u_r + \epsilon_{\tan}(u_\theta u_\theta + u_\phi u_\phi)]. \tag{1}$$

Here ϵ_{rad} and $\epsilon_{\tan}$ represent the radial and tangential components of the permittivity. The radius of spherical geometry is represented by a_1 whereas the radius of core is a_2. An external electric field $\mathbf{E} = \hat{z}E_0 \exp(ikx)$ is applied to the spherical geometry. It is assumed that wavelength (λ) of the externally applied field is much greater than the size of the spherical geometry, i.e., $\lambda \gg a_1$. Such an assumption enables us to study the problem through quasi-static treatment. Under quasi-static approximation, the concept of potential may be introduced through the relations.

$$\nabla \cdot (\bar{\bar{\epsilon}} \cdot \nabla\Phi) = 0 : \quad \text{for homogeneous and anisotropic medium} \tag{2}$$

$$\nabla^2\Phi = 0 : \quad \text{for homogeneous and isotropic medium} \tag{3}$$

In order to incorporate the solution of the above equation, the geometry is divided into three regions. The following is expressions for the potential in each region.

$$\Phi_0(r,\theta) = -E_0 r\cos\theta + Ar^{-2}\cos\theta = \Phi_0^{app} + \Phi_0^{dis}, \qquad r > a_1, \tag{4}$$

$$\Phi_1(r,\theta) = -Br^{\nu}\cos\theta + Cr^{-\nu-1}\cos\theta, \qquad a_1 < r < a_2, \tag{5}$$

$$\Phi_2(r,\theta) = -Dr\cos\theta, \qquad r < a_2. \tag{6}$$

where $\Phi_2(r,\theta)$, $\Phi_1(r,\theta)$, and $\Phi_0(r,\theta)$ are the potentials within the core, shell, and host regions, respectively. Φ_0^{app} and Φ_0^{dis} are respectively applied potential and disturbance potential due to the presence of the spherical geometry. The unknown coefficients A, B, C, D can be determined by imposing the boundary conditions. Parameter ν is written below [26]

$$\nu = \frac{1}{2}\left(-1 \pm \sqrt{1 + 8(\epsilon_{\tan}/\epsilon_{rad})}\right). \tag{7}$$

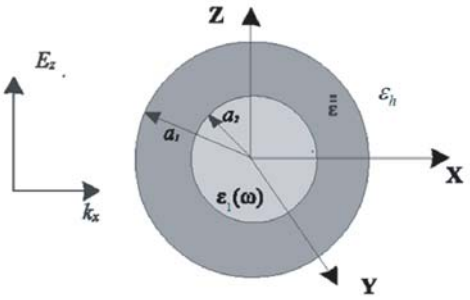

Figure 1. Plasmonic sphere coated with layer of anisotropic dielectric medium.

3. BOUNDARY CONDITIONS

Tangential components of the electric fields are continuous at $r = a_1$ and $r = a_2$, thus the following conditions on potentials are applied

$$\Phi_0 = \Phi_1, \qquad r = a_1, \tag{8}$$

$$\Phi_1 = \Phi_2, \qquad r = a_2. \tag{9}$$

Continuity of normal components of the electric flux densities yields following conditions on potentials

$$\epsilon_h \frac{\partial}{\partial r}\Phi_0 = \epsilon_{rad} \frac{\partial}{\partial r}\Phi_1, \qquad r = a_1, \tag{10}$$

$$\epsilon_{rad} \frac{\partial}{\partial r}\Phi_1 = \epsilon_1 \frac{\partial}{\partial r}\Phi_2, \qquad r = a_2. \tag{11}$$

Algebraic equations obtained from above boundary conditions may be written in matrix form as written below

$$\begin{pmatrix} a_1^{-3} & a_1^{\nu-1} & -a_1^{-\nu-2} & 0 \\ 0 & -a_2^{\nu-1} & a_2^{-\nu-2} & 1 \\ -2\epsilon_h a_1^{-3} & \epsilon_2 \nu a_1^{\nu-1} & \epsilon_2 a_1^{-\nu-2}(\nu+1) & 0 \\ 0 & -\epsilon_2 \nu a_2^{\nu-1} & -\epsilon_2 a_2^{-\nu-2}(\nu+1) & \epsilon_1 \end{pmatrix} \begin{bmatrix} A \\ B \\ C \\ D \end{bmatrix} = \begin{bmatrix} E_0 \\ 0 \\ E_0\epsilon_h \\ 0 \end{bmatrix}. \tag{12}$$

By solving the above matrix equation, the potentials for each region of the geometry are obtained as given below.

$$\Phi_0(r,\theta) = -E_0 r\cos\theta + E_0 \frac{(-\epsilon_1 - \nu\epsilon_{rad} - \epsilon_{rad})(\epsilon_h - \epsilon_{rad}) + \beta(\epsilon_h + \epsilon_{rad} + \nu\epsilon_{rad})(\epsilon_1 - \epsilon_{rad})}{(\epsilon_1 + \epsilon_{rad} + \nu\epsilon_{rad})(\epsilon_{rad} + 2\epsilon_h) - \beta(2\epsilon_h - \epsilon_{rad} - \nu\epsilon_{rad})(\epsilon_1 - \epsilon_{rad})} a_1^3 r^{-2}\cos\theta, \tag{13}$$

$$\Phi_1(r,\theta) = -E_0 \frac{3a_1^{1-\nu}\epsilon_h \nu a_1((-1+a_2^{1+2\nu})\epsilon_1 a_2\nu - \epsilon_2((1+\nu)a_2\nu + a_2^{2+\nu}a_2^{\nu}\nu))}{(\epsilon_1 + \epsilon_{rad} + \nu\epsilon_{rad})(\epsilon_{rad} + 2\epsilon_h) - \beta(2\epsilon_h - \epsilon_{rad} - \nu\epsilon_{rad})(\epsilon_1 - \epsilon_{rad})} r\cos\theta, \tag{14}$$

$$\Phi_2(r,\theta) = -E_0 \frac{a_2^{\nu}[3\epsilon_{rad}(2+\nu)]}{a_2[(\epsilon_1 + \epsilon_{rad} + \nu\epsilon_{rad})(\epsilon_{rad} + 2\epsilon_h) - \beta(2\epsilon_h - \epsilon_{rad} - \nu\epsilon_{rad})(\epsilon_1 - \epsilon_{rad})]} r\cos\theta. \tag{15}$$

where $\beta = (\frac{a_2}{a_1})^{1+2\nu}$. The polarizability P_0 of the spherical geometry can be obtained by comparing with Φ_0^{dis} [27]

$$\Phi_0^{dis} = \frac{1}{4\pi\epsilon_h} P_0 r^{-2}\cos\theta. \tag{16}$$

The polarizability of the spherical geometry is obtained as

$$P_0 = 4\pi\epsilon_h a_1^3 \frac{(-\epsilon_1 - \nu\epsilon_{rad} - \epsilon_{rad})(\epsilon_h - \epsilon_{rad}) + \beta(\epsilon_h + \epsilon_{rad} + \nu\epsilon_{rad})(\epsilon_1 - \epsilon_{rad})}{(\epsilon_1 + \epsilon_{rad} + \nu\epsilon_{rad})(\epsilon_{rad} + 2\epsilon_h) - \beta(2\epsilon_h - \epsilon_{rad} - \nu\epsilon_{rad})(\epsilon_1 - \epsilon_r ad)}. \tag{17}$$

The scattering, absorption and extinction cross-section can be written as given [27].

$$\sigma_{sca} = \frac{1}{6\pi} k^4 |P_0|^2 \tag{18}$$

$$\sigma_{abs} = \frac{k}{\epsilon_h} \mathrm{Im}(P_0) \tag{19}$$

$$\sigma_{ext} = \sigma_{abs} + \sigma_{sca} \tag{20}$$

where k is the wavenumber of the surrounding medium. In order to verify the accuracy of our calculations, corresponding expressions for a special case dealing with the metallic sphere coated with the isotropic dielectric medium are obtained. For this purpose, $\epsilon_{\tan} = \epsilon_{rad} = \epsilon_1$ is substituted in Equations (13)–(15). It may be noted that under this substitution, ν becomes equal to one. For each region of the spherical geometry, expressions for potential are obtained as given below.

$$\Phi_0(r,\theta) = -E_0 r\cos\theta + E_0 \frac{(\epsilon_1 - \epsilon_0)(\epsilon_2 + 2\epsilon_1) + \beta(\epsilon_0 + 2\epsilon_1)(\epsilon_2 - \epsilon_1)}{(\epsilon_1 + 2\epsilon_0)(\epsilon_2 + 2\epsilon_1) + 2\beta(\epsilon_1 - \epsilon_0)(\epsilon_2 - \epsilon_1)} r^{-2}\cos\theta, \tag{21}$$

$$\Phi_1(r,\theta) = -E_0\frac{-3\epsilon_0(\epsilon_2+2\epsilon_1)+3\epsilon_0(\epsilon_2-\epsilon_1)a_2^3r^{-2}}{(\epsilon_1+2\epsilon_0)(\epsilon_2+2\epsilon_1)+2\beta(\epsilon_1-\epsilon_0)(\epsilon_2-\epsilon_1)}r\cos\theta, \tag{22}$$

$$\Phi_2(r,\theta) = -E_0\frac{3\epsilon_0 3\epsilon_1}{(\epsilon_1+2\epsilon_0)(\epsilon_2+2\epsilon_1)+2\beta(\epsilon_1-\epsilon_0)(\epsilon_1-\epsilon_2)}r\cos\theta. \tag{23}$$

The result is the same as that obtained by Sihvola and Lindell [27]. The LD model mathematically manages the frequency dependent characteristics of metals [28], and mathematical expression for the model is written below [29]

$$\epsilon(\omega) = 1 - \frac{f_0\omega_p^2}{\omega(\omega-i\gamma_0)} + \sum_{j=1}^{m}\frac{f_j\omega_P^2}{(\omega_j^2-\omega^2)+i\omega\gamma_j} \tag{24}$$

where ω_p is the plasma frequency of the bulk material, γ_j the decaying constant for j^{th} oscillator, and f_j the oscillator strength. The number of oscillators is taken $m = 5$. The values of different parameters used to obtain behaviors are given in Table 1 [29].

Table 1. Values of different parameters used in LD model for three metals.

parameters (eV)	Tungsten (W)	Silver (Ag)	Gold (Au)
ω_p	13.22	9.01	9.03
f_0	0.206	0.845	0.760
γ_0	0.064	0.048	0.053
f_1	0.054	0.065	0.024
γ_1	0.530	3.886	0.241
ω_1	1.004	0.816	0.415
f_2	0.166	0.124	0.010
γ_2	1.281	0.452	0.345
ω_2	1.917	4.481	0.830
f_3	0.706	0.011	0.071
γ_3	3.332	0.065	0.870
ω_3	3.580	8.185	2.969
f_4	2.590	0.840	0.601
γ_4	5.836	0.916	2.494
ω_4	7.498	9.083	4.304
f_5	—	5.646	4.384
γ_5	—	2.419	2.214
ω_5	—	20.29	13.32

The behavior of dielectric function $\epsilon(\omega) = \epsilon_R(\omega) + i\epsilon_I(\omega)$ for three different metals obtained using LD model is shown in Equation (24). Figure 2 shows the dielectric function plots for W, Ag, and Au for wavelength range (800 nm to 3000 nm). Dielectric function plays a massive role for finding polarization, scattering cross section, absorption, and extinction cross section of these metals. Figure 2 indicates both real and imaginary dielectric functions. It is notified that the real and imaginary dielectric functions are positive and negative for all the three metals through the wavelength range.

4. NUMERICAL RESULTS AND DISCUSSION

The mathematical expressions derived in Section 2 are used to investigate the behavior of optical properties, with respect to the operating wavelength ranging from 800 nm to 3000 nm, of the spherical

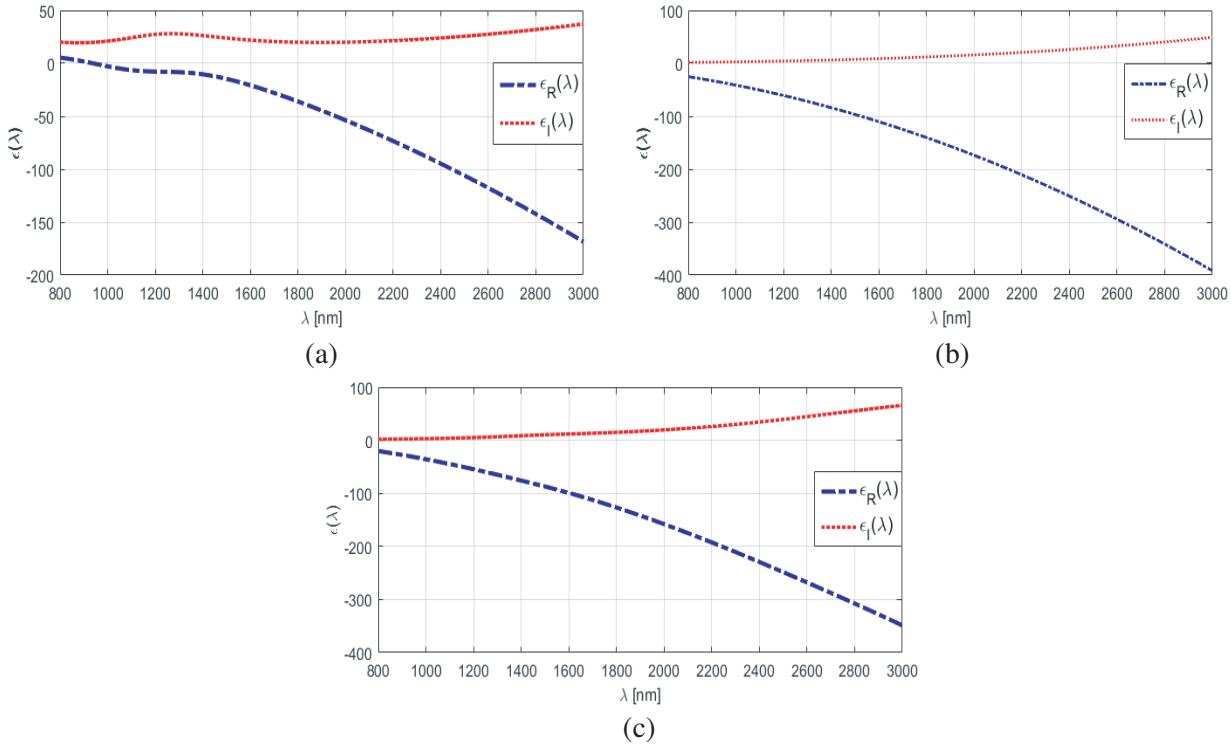

Figure 2. Behavior of dielectric function for tungsten, silver, and gold metals. (a) Tungsten. (b) Silver. (c) Gold.

Table 2. Shift in surface plasmon resonance due to variation of core radius. $a_1 = 160\,\text{nm}$, $\epsilon_{rad} = 27$ and $\epsilon_{\tan} = 21$.

Metal	Range of a_2	Shift in P_{real}	Shift in P_{imag}	Shift in σ_{sca}	Shift in σ_{abs}	Shift in σ_{ext}
Tungsten	100 to 145 nm	110 nm	110 nm	115 nm	100 nm	120 nm
Silver	100 to 145 nm	130 nm	120 nm	120 nm	115 nm	115 nm
Gold	100 to 145 nm	130 nm	110 nm	110 nm	115 nm	115 nm

geometry. For this purpose, plots for polarizability, absorption, scattering, and extinction cross sections are used. For analysis, throughout the discussion three different metals (tungsten, silver, and gold) are taken for core of the spherical geometry, but one is considered at a time. Coating of anisotropic dielectric material is taken, and the surrounding medium has scalar permittivity $\epsilon_h = 14$. Our objective is to explore the role and impact of anisotropy on the optical properties when radius of the geometry is either kept constant or varied. In this regard, the discussion is divided into two main parts. In the first part, the effect of variation of core radius a_1 or radius a_2 of spherical geometry is noted. Values for radial and tangential components of anisotropic permittivity are taken $\epsilon_{rad} = 27$ or $\epsilon_{\tan} = 21$ for this part. In the second part, the impact of variation of radial and tangential components of the anisotropy is studied taking $a_1 = 160\,\text{nm}$ and $a_2 = 100\,\text{nm}$. It may be noted that values of the anisotropic permittivity used in this paper are taken from [30].

Impacts on polarizability, scattering cross sections, absorption, and extinction cross section for tungsten metal by varying a_2 or a_1 are shown in Figures 3–5. Figures 3(a) & (b) contain real and imaginary parts of the polarizability when a_2 is varied whereas Figures 3(c) & (d) contain plots for polarizability when a_1 is varied. For first part of the discussion, $a_1 = 160\,\text{nm}$ and $a_2 = 100, 115, 130, 145\,\text{nm}$ or $a_2 = 100\,\text{nm}$ and $a_1 = 115, 130, 145, 160\,\text{nm}$ are considered for analysis. The impact of variation of a_2 and a_1 on the scattering cross section, absorption, and extinction cross

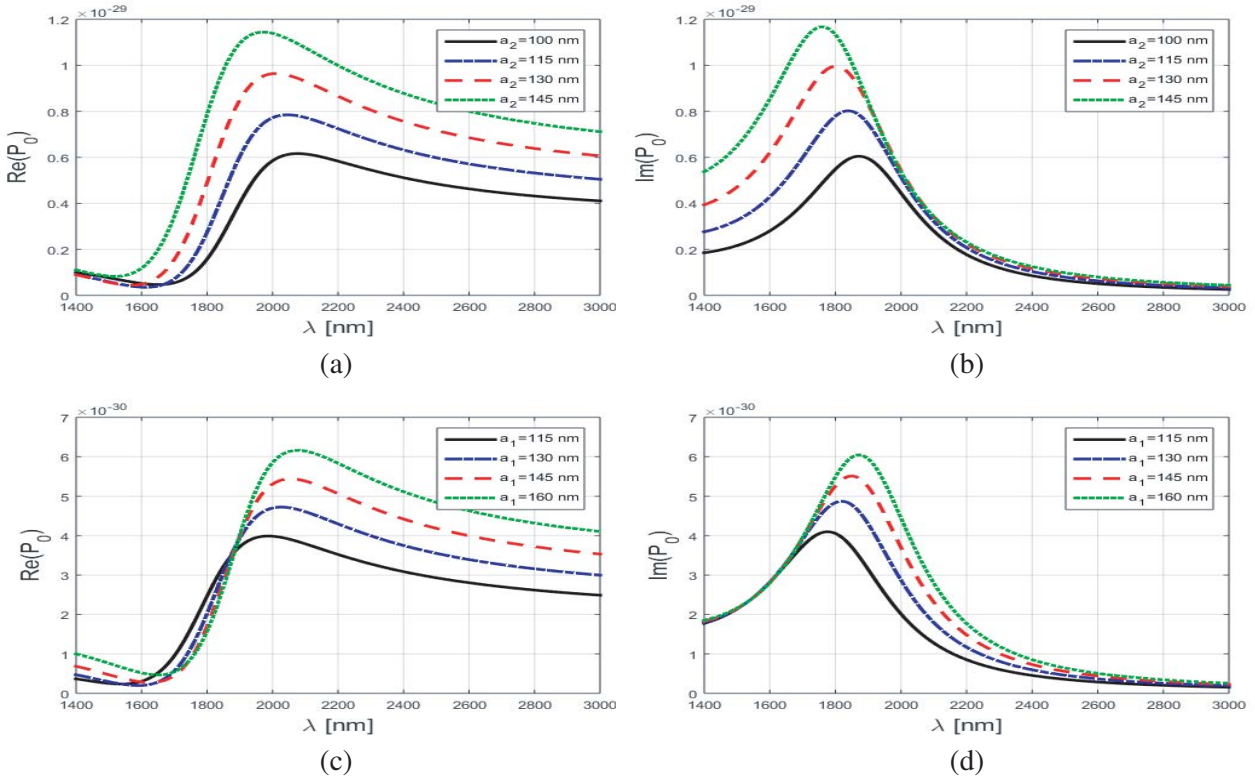

Figure 3. Behavior of real and imaginary parts of polarizability for tungsten metal with respect to operating wavelength Figures 3(a) & (b) for specific values of a_2, Figures 3(c) & (d) for specific values of a_1.

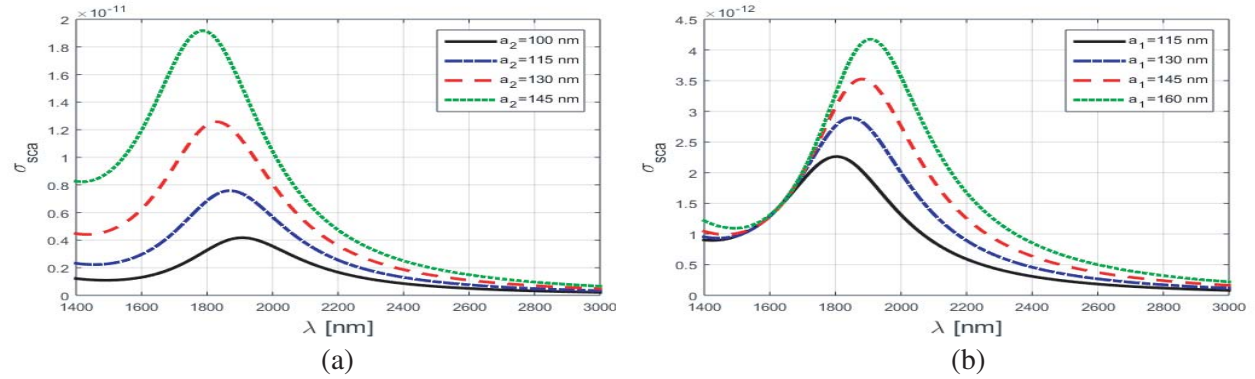

Figure 4. Behavior of scattering cross-section for tungsten metal with respect to operating wavelength. Figure 4(a) for specific values of a_2, Figure 4(b) for specific values of a_1.

Table 3. Shift in surface plasmon resonance due to variation of radius of spherical geometry. $a_2 = 100\,\text{nm}$, $\epsilon_{rad} = 27$ and $\epsilon_{\tan} = 21$.

Metal	Range of a_1	Shift in P_{real}	Shift in P_{imag}	Shift in σ_{sca}	Shift in σ_{abs}	Shift in σ_{ext}
Tungsten	115 to 160 nm	105 nm	95 nm	100 nm	90 nm	110 nm
Silver	115 to 160 nm	110 nm	105 nm	140 nm	140 nm	140 nm
Gold	115 to 160 nm	110 nm	100 nm	100 nm	95 nm	100 nm

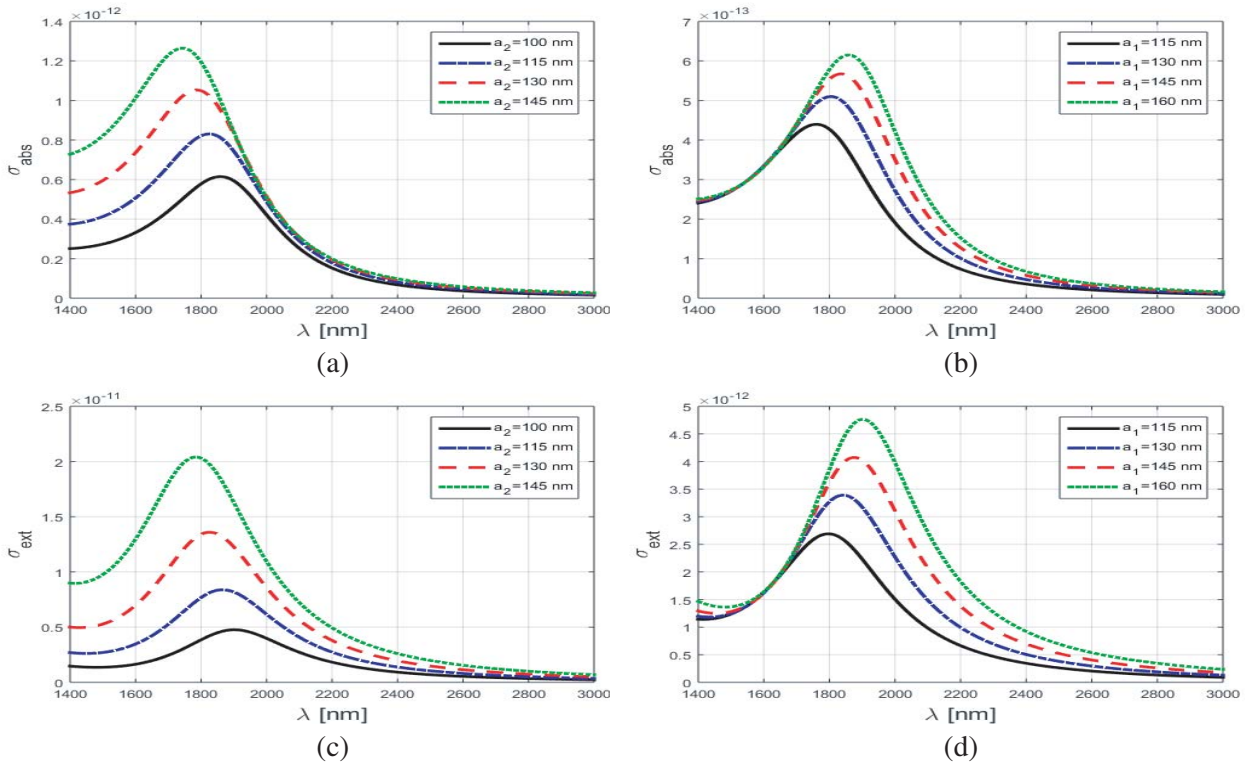

Figure 5. Behavior of absorption and extinction cross-section for tungsten metal with respect to operating wavelength for specific values of a_2 and a_1.

section is plotted in Figures 4(a) & (b), Figures 5(a) & (b) and Figures 5(c) & (d), respectively. It is noted in Figures 3–5 that the increase in radius of core a_2 by 45 nm causes the shift in the position of peak values of polarizability, scattering cross section, absorption, and extinction cross sections towards shorter wavelength by 110 nm, 115 nm, 100 nm, and 120 nm, respectively. The variation in a_1 causes the shift of 95 nm, 100 nm, 90 nm, and 110 nm towards longer wavelengths in peak values of polarizability, scattering cross sections, absorption, and extinction cross section. Moreover, it is also observed that the increase in radius of the core or spherical geometry increases the magnitudes of peak values of P_0, σ_{sca}, σ_{abs}, and σ_{ext} for tungsten metal. The behaviors of polarizability, scattering, absorption, and extinction cross sections for silver and gold are depicted in Figures 6–11. The shift in peak values of P_0, σ_{sca}, σ_{abs}, and σ_{ext} toward short and long wavelengths is observed for variation in specific values of a_2 and a_1. The peak values of P_0, σ_{sca}, σ_{abs}, σ_{ext} for silver and gold metals are shifted by 120 nm, 120 nm, 115 nm, 115 nm and 110 nm, 110 nm, 115 nm, 115 nm towards short wavelengths, respectively. The variation of a_1 shifts the peak values of P_0, σ_{sca}, σ_{abs}, σ_{ext} 105 nm, 140 nm, 140 nm, 140 nm and 100 nm, 100 nm, 95 nm, 100 nm towards longer wavelengths for silver and gold metals, respectively. The variation in a_2 causes increases in peak values of P_0, σ_{sca}, σ_{abs}, σ_{ext} for silver and gold. The increase in peak values of P_0 and σ_{abs} is noted as a_1 is varied, and the decrease in magnitude of peak values of σ_{sca} and σ_{ext} is observed for silver and gold. The shift in surface plasmon resonance location for P_0, σ_{sca}, σ_{abs}, σ_{ext} is listed in Table 2 and Table 3.

In the second part of discussion, behaviors of polarizability, scattering cross sections, absorption, and extinction cross sections taking different specific values of the components of anisotropic parameter are presented and shown in Figures 12–19. For these plots, ϵ_{rad} = 18, 21, 24, 27 and $\epsilon_{\tan}$ = 21 or ϵ_{rad} = 21 and $\epsilon_{\tan}$ = 18, 21, 24, 27 are considered. Now radii of both core and spherical geometry are kept constant as a_2 = 100 nm and a_1 = 160 nm. The shift of (85 nm, 80 nm, 75 nm, 95 nm) for tungsten, (75 nm, 75 nm, 75 nm, 75 nm) for silver and (75 nm, 80 nm, 80 nm, 75 nm) for gold in peak values of P_0, σ_{sca}, σ_{abs}, σ_{ext}, respectively towards longer wavelengths is noted due to variation in specific values of $\epsilon_{\tan}$. The increase in magnitude of polarizability, scattering cross sections, absorption, and extinction cross

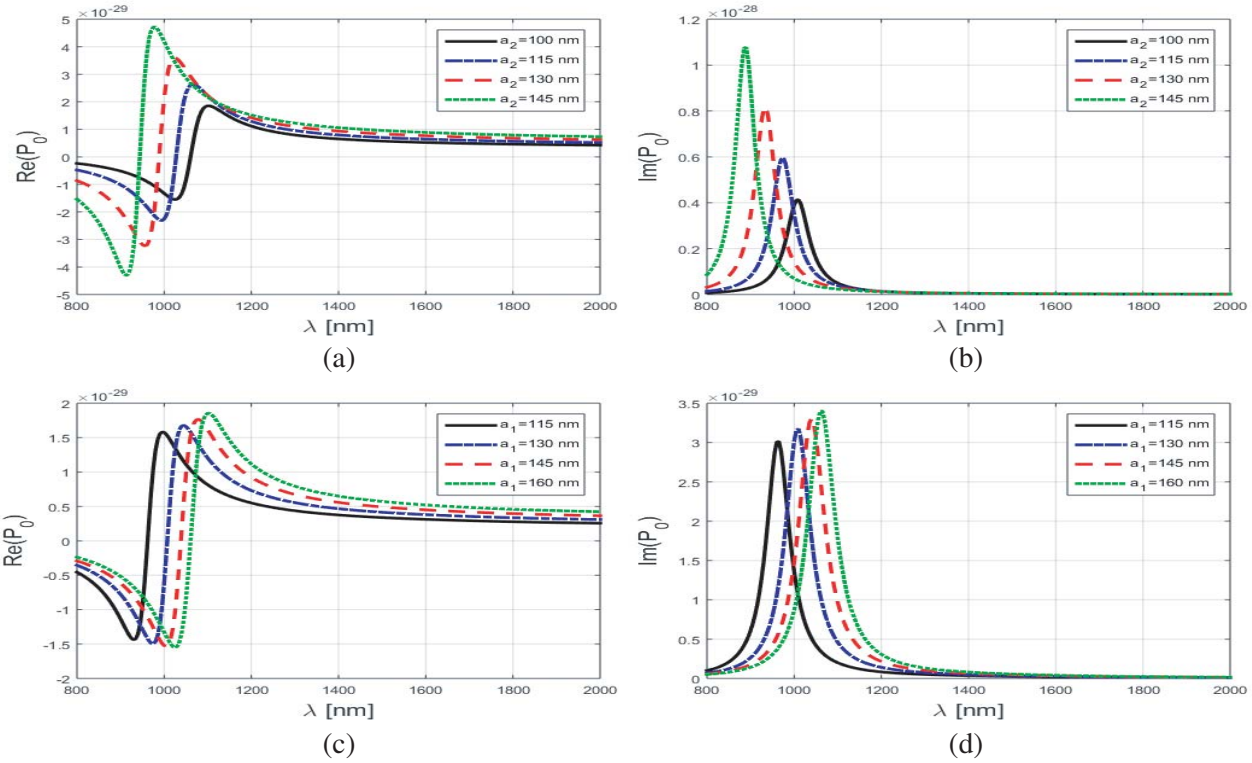

Figure 6. Behavior of real and imaginary parts of polarizability for silver metal with respect to operating wavelength. Figures 6(a) & (b) for specific values of a_2, Figures 6(c) & (d) for specific values of a_1.

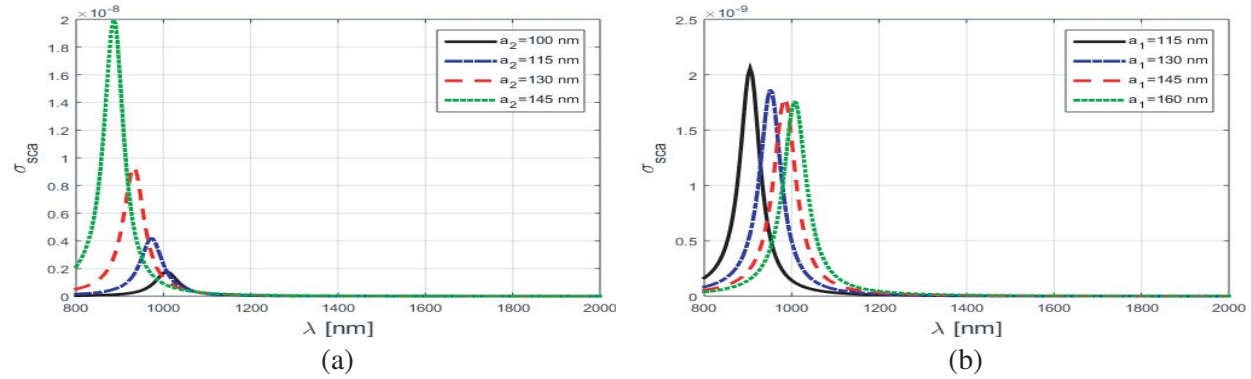

Figure 7. Behavior of scattering cross-section for silver metal with respect to operating wavelength. Figure 7(a) for specific values of a_1 and Figure 7(b) for a_2.

section is also observed. Similarly, the peak value of optical properties towards the longer wavelength is observed as ϵ_{rad} is varied for specific values. The shift in the location of peak values of P_0, σ_{sca}, σ_{abs}, σ_{ext} is observed as (65 nm, 65 nm, 80 nm, 45 nm) for tungsten metal, (60 nm, 60 nm, 60 nm, 45 nm) for silver metal, and (55 nm, 55 nm, 50 nm, 55 nm) for gold metal is observed. However, the decrease in peak values of polarizability, scattering cross sections, absorption, and extinction cross section is also noted. It is noticed that the location and magnitude of surface plasmon resonance may be adjusted accordingly by selecting the appropriate values of parameters of the geometry. The shift in surface plasmon resonance location for P_0, σ_{sca}, σ_{abs}, and σ_{ext} is listed in Table 4 and Table 5 for variation in both anisotropic parameters.

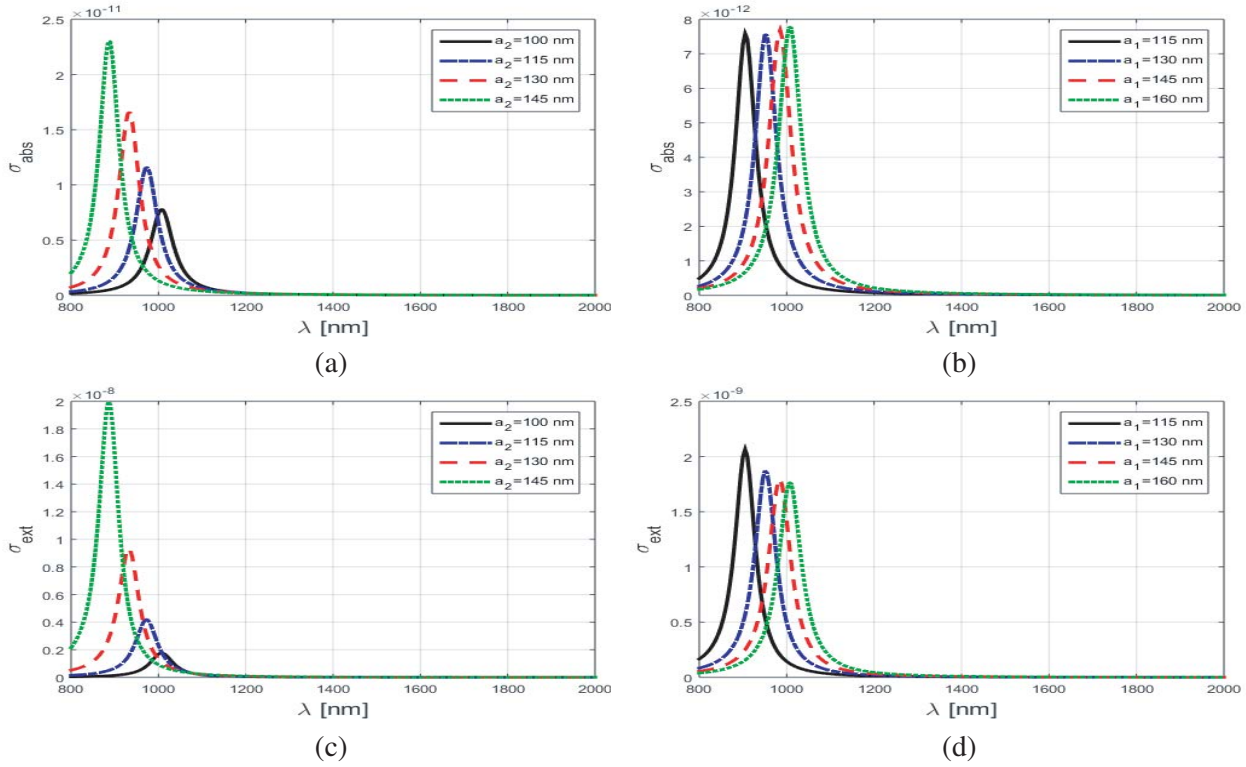

Figure 8. Behavior of absorption and extinction cross-section of silver metal for specific values of a_1 and a_2.

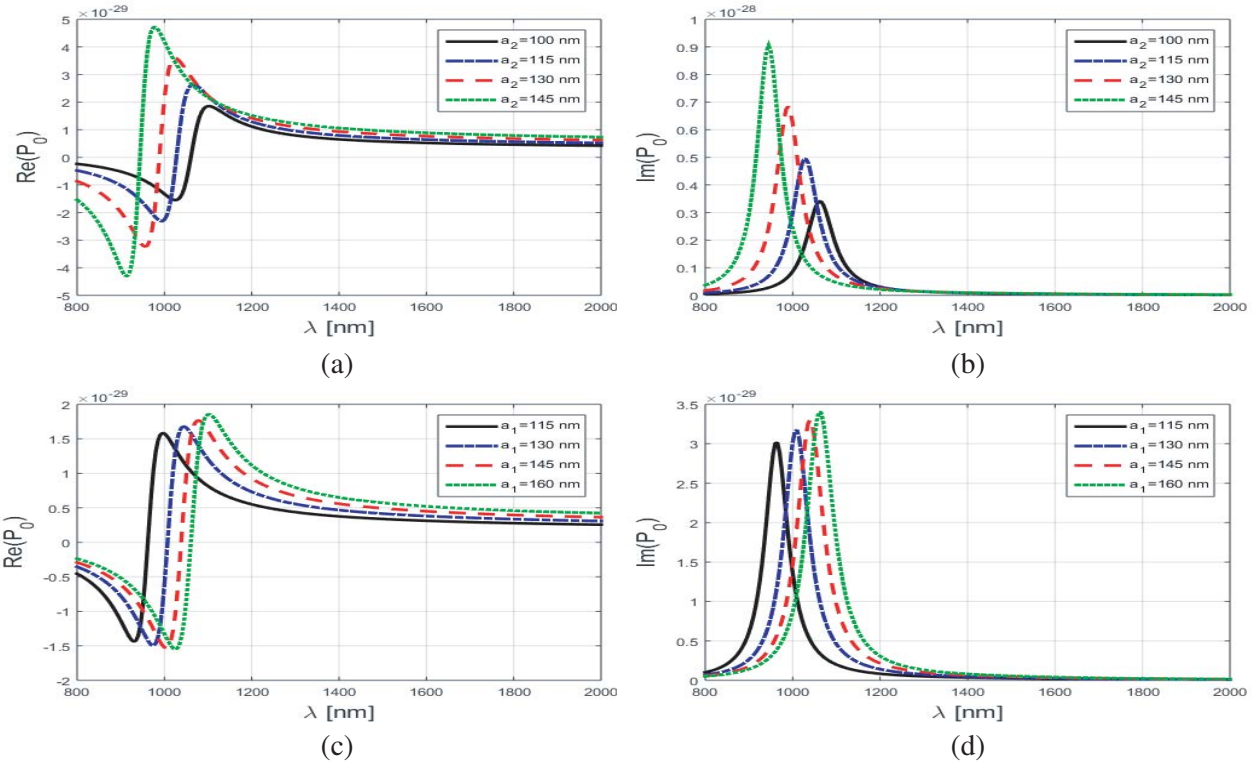

Figure 9. Behavior of real and imaginary parts of polarizability for gold metal with respect to operating wavelength. Figures 9(a) & (b) for specific values of a_2, Figures 9(c) & (d) for specific values of a_1.

Table 4. Shift in surface plasmon resonance due to variation of tangential component, $a_1 = 160$, $a_2 = 100\,\text{nm}$ and $\epsilon_{rad} = 27$.

Metal	Range of $\epsilon_{\tan}$	Shift in P_{real}	Shift in P_{imag}	Shift in σ_{sca}	Shift in σ_{abs}	Shift in σ_{ext}
Tungsten	18 to 27	50 nm	65 nm	65 nm	80 nm	45 nm
Silver	18 to 27	65 nm	60 nm	60 nm	60 nm	45 nm
Gold	18 to 27	65 nm	55 nm	55 nm	50 nm	55 nm

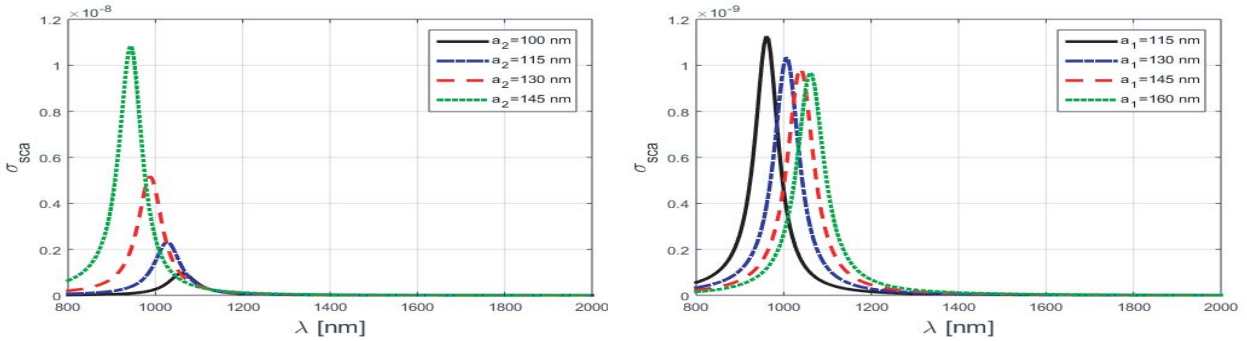

Figure 10. Behavior of scattering cross-section for gold metal with respect to operating wavelength. Figure 10(a) for specific values of a_2, Figure 10(b) for specific values of a_1.

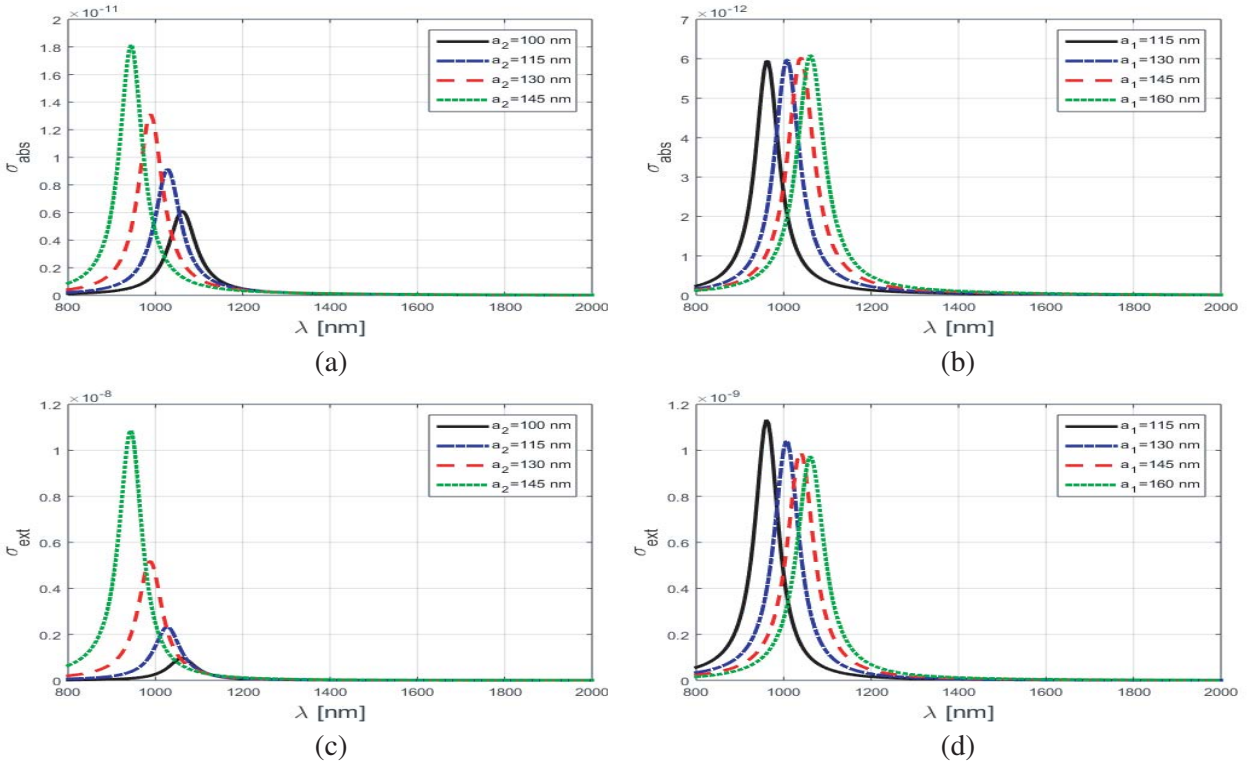

Figure 11. Behavior of absorption in Figures 11(a) & (b) and extinction cross-section in Figures 11(c) & (d) for gold metal for specific values of a_1 and a_2.

Table 5. Shift in surface plasmon resonance due to variation of radial component, $a_1 = 160\,\text{nm}$, $a_2 = 100\,\text{nm}$ and $\epsilon_{\tan} = 21$.

Metal	Range of ϵ_{rad}	Shift in P_{real}	Shift in P_{imag}	Shift in σ_{sca}	Shift in σ_{abs}	Shift in σ_{ext}
Tungsten	18 to 27	80 nm	85 nm	80 nm	75 nm	95 nm
Silver	18 to 27	85 nm	75 nm	75 nm	75 nm	75 nm
Gold	18 to 27	80 nm	75 nm	80 nm	80 nm	75 nm

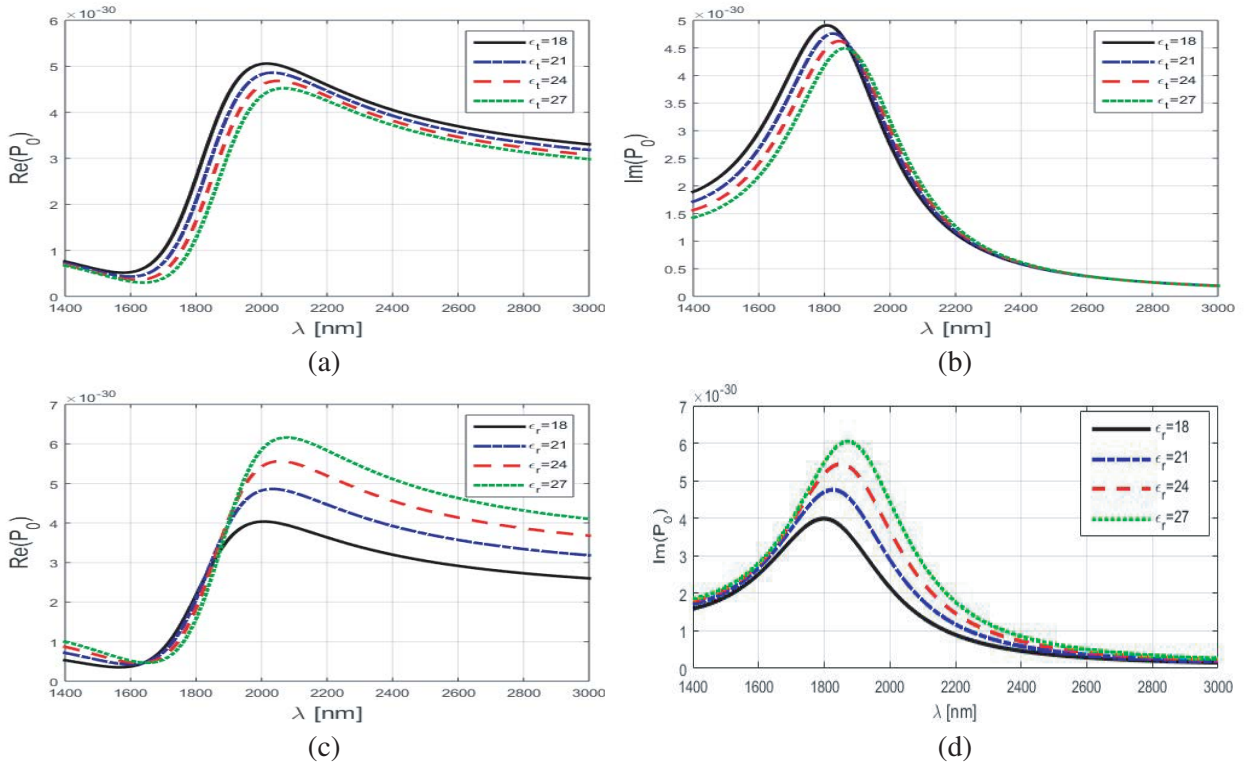

Figure 12. Behavior of real and imaginary parts of polarizability for tungsten metal with respect to operating wavelength for specific values of ϵ_{rad} or $\epsilon_{\tan}$.

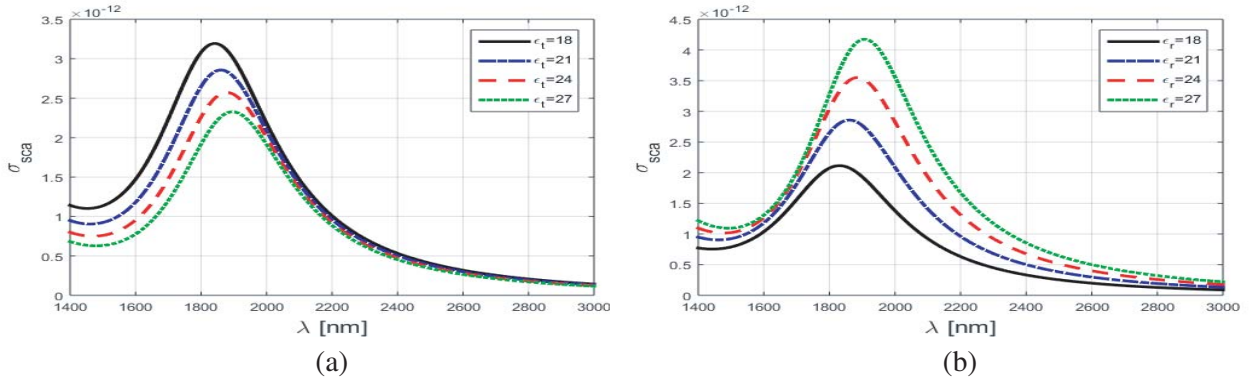

Figure 13. Behavior of scattering cross section of tungsten metal for specific values of ϵ_{rad} and $\epsilon_{\tan}$.

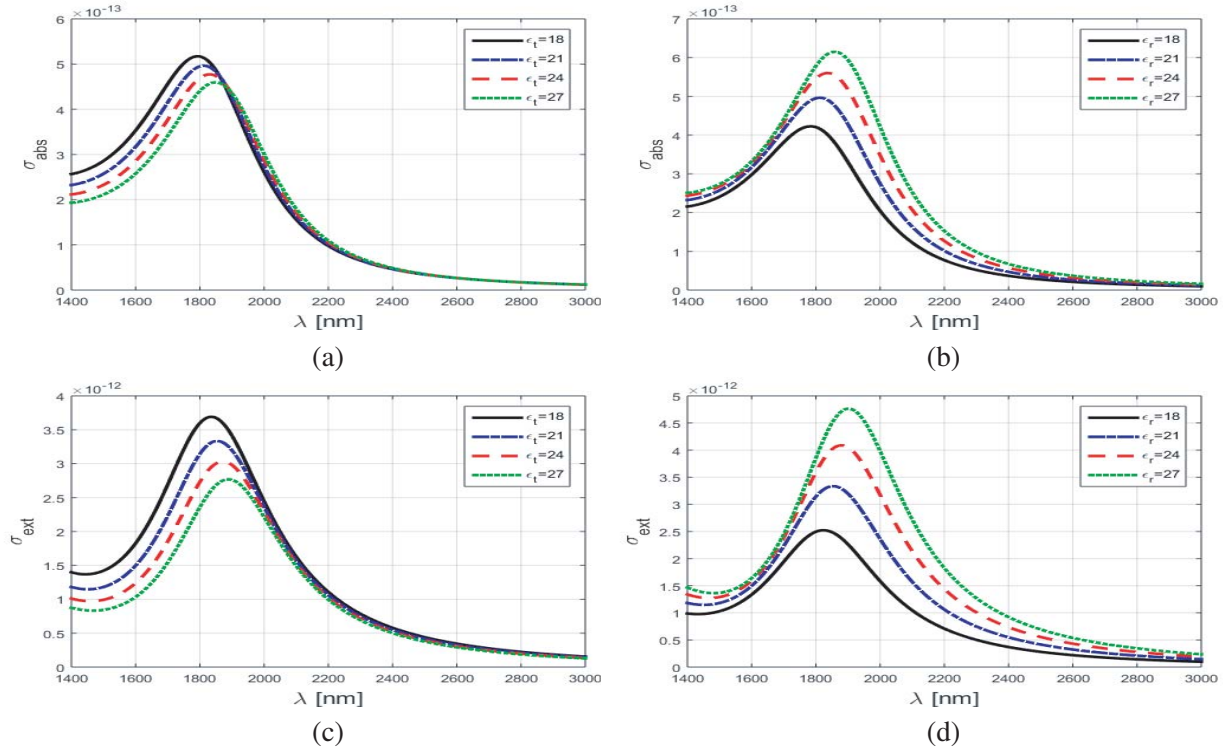

Figure 14. Behavior of absorption and extinction cross section of tungsten metal for specific values of ϵ_{rad} and $\epsilon_{\tan}$.

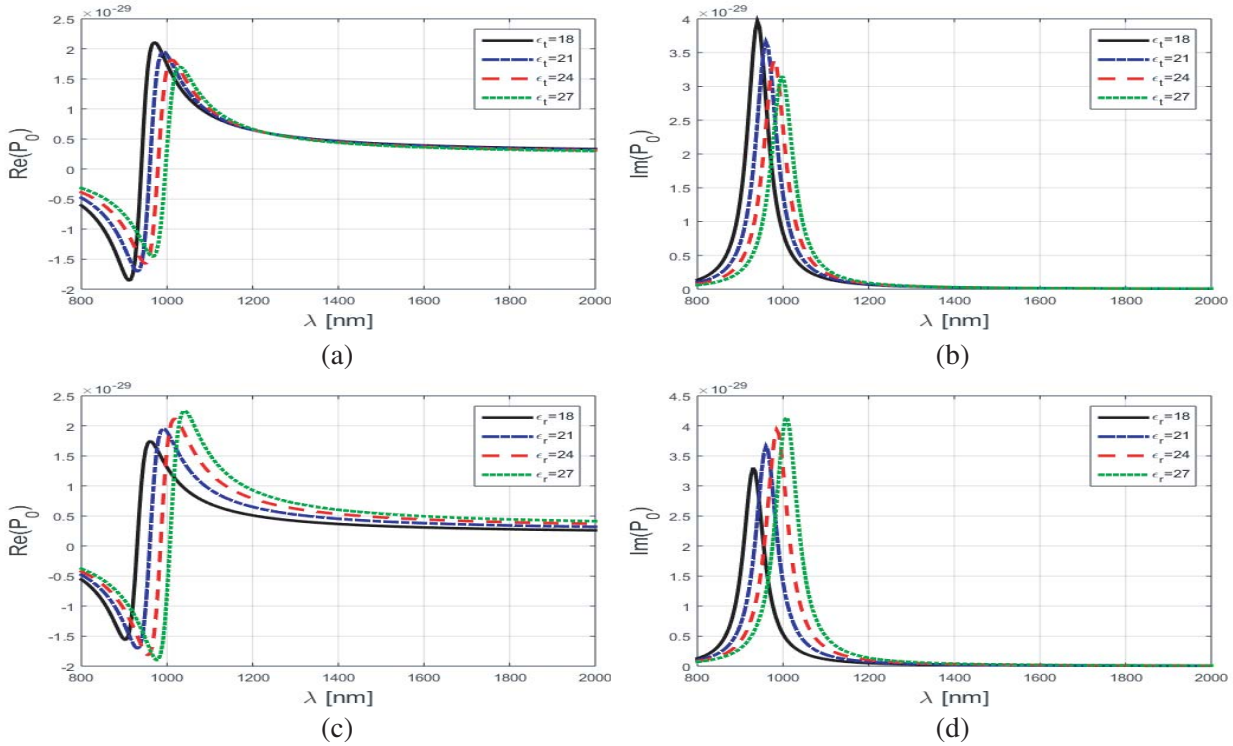

Figure 15. Behavior of real and imaginary parts of polarizability for silver metal with respect to operating wavelength Figures 18(a) & (b) for specific values of $\epsilon_{\tan}$ and Figures 18(c) & (d) for specific values of ϵ_{rad}.

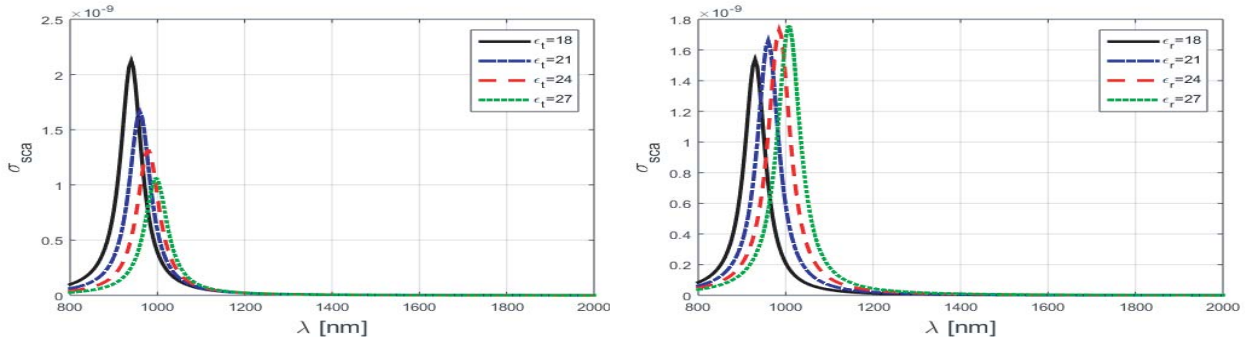

(a) (b)

Figure 16. Behavior of scattering cross-section for silver metal with respect to operating wavelength for specific values of ϵ_{rad} or $\epsilon_{\tan}$.

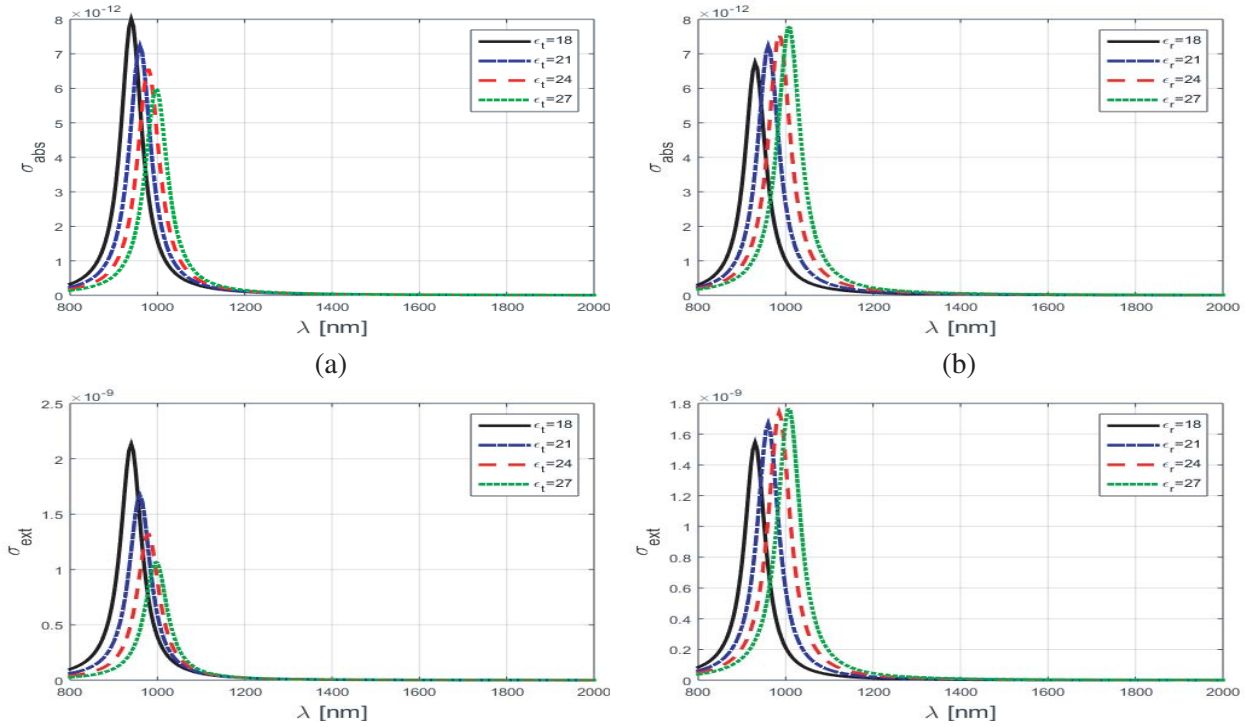

(a) (b)

(c) (d)

Figure 17. Behavior of absorption and extinction cross-section of silver metal for specific values of $\epsilon_{\tan}$ and ϵ_{rad}.

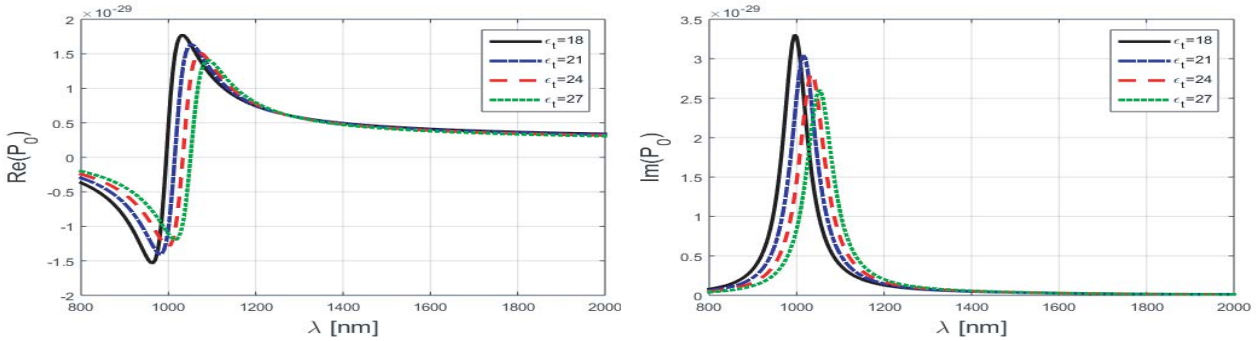

(a) (b)

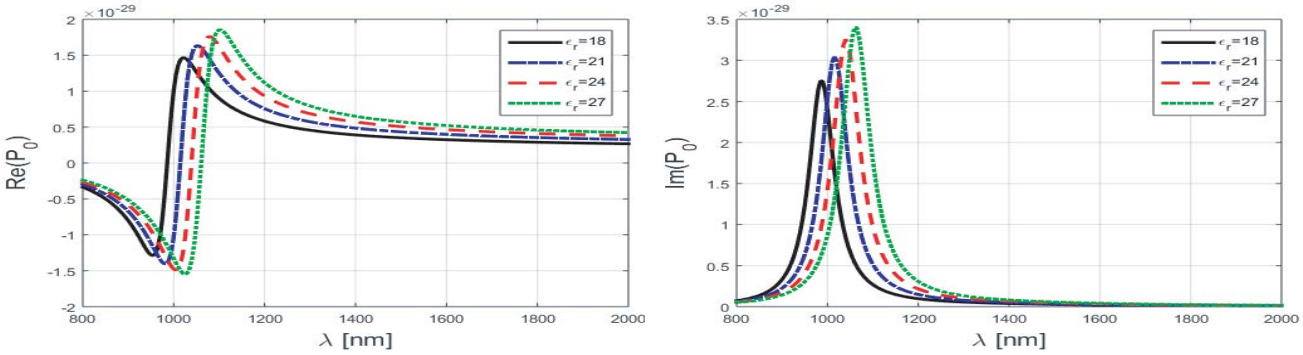

Figure 18. Behavior of real and imaginary parts of polarizability for gold metal with respect to operating wavelength Figures 19(a) & (b) for specific values of $\epsilon_{\tan}$ and Figures 19(c) & (d) for specific values of ϵ_{rad}.

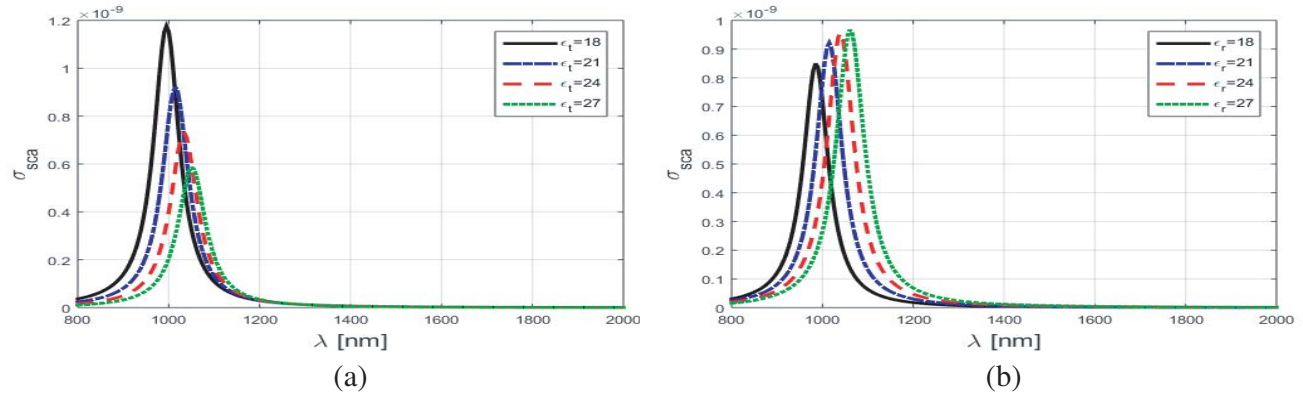

Figure 19. Behavior of scattering cross-section for gold metal with respect to operating wavelength for specific values of ϵ_{rad} or $\epsilon_{\tan}$.

5. CONCLUSIONS

The optical properties of a nano-metallic particle coated with radially anisotropic dielectric medium is studied. For this purpose, the behaviors of polarizability, scattering, absorption, and extinction cross sections are plotted. Due to the increase in radius of core of geometry rise in peak value of polarizability, scattering, absorption, extinction cross section, and shift in its location towards the shorter wavelengths are observed. On the other hand, the shift in location of polarizability, scattering, absorption, and extinction cross section towards longer wavelength is noted as radius of spherical geometry is increased. The increase in peak value of polarizability is observed for all three metals, but the decrease in peak value of scattering cross section for (silver/gold) is noted. Shift in the location of peak value of polarizability, absorption, scattering, and extinction cross section towards longer wavelengths for the increase in both radial or tangential components of tensor permittivity of spherical geometry is noted. The increase in their peak value is noted due to the increase in value of radial component of permittivity, and the decrease in peak value is observed for increase in tangential component of permittivity. The impact of increase of radial component of permittivity is more significant than corresponding tangential component of permittivity.

REFERENCES

1. Mie, G., "Beiträge zur optik truber medien, speziell kolloidaler metallösungen," *Annalen der Physik*, Vol. 330, No. 3, 377–445, 1908.
2. Yoon, T.-J., K. N. Yu, E. Kim, J. S. Kim, B. G. Kim, S.-H. Yun, B.-H. Sohn, M.-H. Cho, J.-K. Lee, and S. B. Park, "Specific targeting, cell sorting, and bioimaging with smart magnetic silica core-shell nanomaterials," *Small*, Vol. 2, No. 2, 209–215, 2006.
3. Chen, G., J. Shen, T. Y. Ohulchanskyy, N. J. Patel, A. Kutikov, Z. Li, J. Song, R. K. Pandey, H. Ågren, P. N. Prasad, et al., "(α-naybf$_4$: Tm_{3+})/caf$_2$ core/shell nanoparticles with efficient near-infrared to near-infrared upconversion for high-contrast deep tissue bioimaging," *ACS Nano*, Vol. 6, No. 9, 8280–8287, 2012.
4. Feng, H. Y., F. Luo, D. Meneses-Rodríguez, G. Armelles, and A. Cebollada, "From disk to ring: Aspect ratio control of the magnetoplasmonic response in Au/Co/Au nanostructures fabricated by hole-mask colloidal lithography," *Applied Physics Letters*, Vol. 106, No. 8, 083105, 2015.
5. Zayats, A. V. and I. I. Smolyaninov, "Near-field photonics: Surface plasmon polaritons and localized surface plasmons," *Journal of Optics A: Pure and Applied Optics*, Vol. 5, No. 4, S16, 2003.
6. Atwater, H. A. and A. Polman, "Plasmonics for improved photovoltaic devices," *Materials for Sustainable Energy: A Collection of Peer-Reviewed Research and Review Articles from Nature Publishing Group*, 1–11, World Scientific, 2011.
7. Anker, J. N., W. P. Hall, O. Lyandres, N. C. Shah, J. Zhao, and R. P. Van Duyne, "Biosensing with plasmonic nanosensors," *Nanoscience and Technology: A Collection of Reviews from Nature Journals*, 308–319, World Scientific, 2010.
8. Pande, S., S. K. Ghosh, S. Praharaj, S. Panigrahi, S. Basu, S. Jana, A. Pal, T. Tsukuda, and T. Pal, "Synthesis of normal and inverted gold-silver coreshell architectures in β-cyclodextrin and their applications in sers," *The Journal of Physical Chemistry C*, Vol. 111, No. 29, 10806–10813, 2007.
9. Kim, J., H. S. Kim, N. Lee, T. Kim, H. Kim, T. Yu, I. C. Song, W. K. Moon, and T. Hyeon, "Multifunctional uniform nanoparticles composed of a magnetite nanocrystal core and a mesoporous silica shell for magnetic resonance and fluorescence imaging and for drug delivery," *Angewandte Chemie International Edition*, Vol. 47, No. 44, 8438–8441, 2008.
10. Lee, K.-S. and M. A. El-Sayed, "Gold and silver nanoparticles in sensing and imaging: Sensitivity of plasmon response to size, shape, and metal composition," *The Journal of Physical Chemistry B*, Vol. 110, No. 39, 19220–19225, 2006.
11. Liedberg, B., C. Nylander, and I. Lunström, "Surface plasmon resonance for gas detection and biosensing," *Sensors and Actuators*, Vol. 4, 299–304, 1983.
12. Verbruggen, S. W., M. Keulemans, J. A. Martens, and S. Lenaerts, "Predicting the surface plasmon resonance wavelength of gold-silver alloy nanoparticles," *The Journal of Physical Chemistry C*, Vol. 117, No. 37, 19142–19145, 2013.
13. Ali, A., Q. A. Naqvi, and M. A. Baqir, "Investigation of the plasmon resonance of core-shell nanoparticle in the near-infrared region," *Journal of Electromagnetic Waves and Applications*, Vol. 33, No. 18, 2462–2475, 2019.
14. Mohapatra, S., Y. Mishra, D. Avasthi, D. Kabiraj, J. Ghatak, and S. Varma, "Synthesis of gold-silicon core-shell nanoparticles with tunable localized surface plasmon resonance," *Applied Physics Letters*, Vol. 92, No. 10, 103105, 2008.
15. Gerislioglu, B., A. Ahmadivand, and N. Pala, "Optothermally controlled charge transfer plasmons in Au-$Ge_2Sb_2Te_5$ core-shell assemblies," arXiv preprint arXiv:1712.01092, 2017.
16. Sukhorukov, V. L., G. Meedt, M. Kurschner, and U. Zimmermann, "A single-shell model for biological cells extended to account for the dielectric anisotropy of the plasma membrane," *Journal of Electrostatics*, Vol. 50, No. 3, 191–204, 2001.
17. Ambjornsson, T., G. Mukhopadhyay, S. P. Apell, and M. Kall, "Resonant coupling between localized plasmons and anisotropic molecular coatings in ellipsoidal metal nanoparticles," *Physical Review B*, Vol. 73, No. 8, 085412, 2006.

18. Pendry, J. B., D. Schurig, and D. R. Smith, "Controlling electromagnetic fields," *Science*, Vol. 312, No. 5781, 1780–1782, 2006.
19. Gao, L., T. Fung, K. Yu, and C. Qiu, "Electromagnetic transparency by coated spheres with radial anisotropy," *Physical Review E*, Vol. 78, No. 4, 046609, 2008.
20. Ni, Y., L. Gao, A. Miroshnichenko, and C. Qiu, "Controlling light scattering and polarization by spherical particles with radial anisotropy," *Optics Express*, Vol. 21, No. 7, 8091–8100, 2013.
21. Nisar, M. and Q. A. Naqvi, "Cloaking and magnifying using radial anisotropy in non-integer dimensional space," *Physics Letters A*, Vol. 382, No. 31, 2055–2060, 2018.
22. Wallén, H., H. Kettunen, and A. Sihvola, "Anomalous absorption, plasmonic resonances, and invisibility of radially anisotropic spheres," *Radio Science*, Vol. 50, No. 1, 18–28, 2015.
23. Kettunen, H., H. Wallén, and A. Sihvola, "Cloaking and magnifying using radial anisotropy," *Journal of Applied Physics*, Vol. 114, No. 4, 044110, 2013.
24. Liu, H.-Z., J. L.-W. Li, M. S. Leong, and S. Zouhdi, "Transparent uniaxial anisotropic spherical particles designed using radial anisotropy," *Physical Review E*, Vol. 84, No. 1, 016605, 2011.
25. Chen, H. and L. Gao, "Tunablity of the unconventional fano resonances in coated nanowires with radial anisotropy," *Optics Express*, Vol. 21, No. 20, 23619–23630, 2013.
26. Reshetnyak, V. Y., I. P. Pinkevych, T. J. Sluckin, and D. R. Evans, "Cloaking by shells with radially inhomogeneous anisotropic permittivity," *Optics Express*, Vol. 24, No. 2, A21–A32, 2016.
27. Sihvola, A. and I. V. Lindell, "Transmission line analogy for calculating the effective permittivity of mixtures with spherical multilayer scatterers," *Journal of Electromagnetic Waves and Applications*, Vol. 2, No. 8, 741–756, 1988.
28. Barchiesi, D. and T. Grosges, "Fitting the optical constants of gold, silver, chromium, titanium, and aluminum in the visible bandwidth," *Journal of Nanophotonics*, Vol. 8, No. 1, 083097, 2014.
29. Rakić, A. D., A. B. Djurišić, J. M. Elazar, and M. L. Majewski, "Optical properties of metallic films for vertical-cavity optoelectronic devices," *Applied Optics*, Vol. 37, No. 22, 5271–5283, 1998.
30. Kettunen, H., H. Wallén, and A. Sihvola, "Tailoring effective media by mie resonances of radially-anisotropic cylinders," *Photonics*, Vol. 2, 509–526, Multidisciplinary Digital Publishing Institute, 2015.